Am J Transl Res 2026;18(6):5492-5510
www.ajtr.org /ISSN:1943-8141/AJTR0172223

Original Article

Progranulin promotes glioma progression through the M2-TGF-β axis: targeted therapy with SORT1-loaded HAMA hydrogel microspheres

He Zhang, Shuai Yuan, Yawen Pan

Lanzhou University Second Hospital, Lanzhou, Gansu, China

Received February 24, 2026; Accepted May 14, 2026; Epub June 25, 2026; Published June 30, 2026

Abstract: Glioblastoma (GBM) is the most aggressive primary brain tumor, and is characterized by rapid growth, therapeutic resistance, and a highly immunosuppressive tumor microenvironment (TME). Progranulin (GRN/PGRN), a secreted glycoprotein, promotes malignancy in various cancers, yet its role in GBM remains poorly defined. Bioinformatics analysis of GEO (Gene Expression Omnibus) and TCGA (The Cancer Genome Atlas) datasets revealed that GRN expression is significantly upregulated in GBM and is associated with shorter overall survival and progression-free survival. High GRN levels correlated strongly with increased M2 macrophage infiltration (marked by CD163 expression) and elevated immune and stromal scores, suggesting that GRN contributes to an immunosuppressive TME. In vitro, silencing GRN in GBM cells markedly inhibited cell proliferation, migration, invasion, and colony formation. Coculture assays demonstrated that GRN knockdown reduced GBM-induced M2 macrophage polarization ($CD206^+$) while increasing M1 polarization ($CD86^+$), accompanied by decreased secretion of the immunosuppressive cytokines IL-10 and TGF-β. Transwell experiments further showed that GRN promoted GBM invasion in a macrophage-dependent manner via the TGF-β pathway, an effect that was abrogated by the TGF-β receptor I inhibitor LY3200882. We developed SORT1-loaded hyaluronic acid methacrylate (HAMA) hydrogel microspheres to target GRN therapeutically. SORT1 competitively binds to GRN, reducing its concentration in the TME. Intratumoral injection of these microspheres significantly suppressed GBM xenograft growth in vivo. Collectively, our findings identify GRN as a key driver of GBM progression and TME immunosuppression through M2 macrophage polarization and TGF-β signaling. Targeting GRN with SORT1-loaded HAMA microspheres represents a promising adjuvant therapeutic strategy for GBM.

Keywords: Glioblastoma, progranulin, M2 macrophage polarization, tumor microenvironment

Introduction

Glioblastoma (GBM) is the most common primary malignant brain tumor in adults, accounting for approximately 14% of all primary brain tumors and over 50% of malignant brain tumors in adults. Its highly invasive growth pattern and pronounced intratumoral heterogeneity not only substantially increase the difficulty of clinical treatment but also constitutes the core reason for the extremely poor prognosis for patients. According to the latest epidemiological data, the median survival time is only 12-15 months, with 2-year survival rates of approximately 18-30% and 5-year survival rates of merely 5-10%, indicating that the current treatment outcomes remain far from satisfactory [1, 2]. GBM is characterized by highly infiltrative growth, a limited responsiveness to conventional therapeutic modalities, and an exceedingly complex tumor microenvironment. These interrelated factors collectively result in its dismal clinical prognosis. Elucidating the intricate cellular and molecular interactions within the tumor microenvironment is essential, as it will lay a critical theoretical foundation for the development of novel, precise, targeted therapeutic strategies [3, 4].

The TME plays a pivotal role in glioma initiation and progression, with tumor-associated macrophages (TAMs) being especially critical. Upon polarization to the protumorigenic M2 phenotype, TAMs secrete factors that increase tumor

https://doi.org/10.62347/RCNF5171

proliferation, invasion, and immune evasion [5]. Recent studies have shown that progranulin (PGRN; gene name: GRN), a secreted glycoprotein, is overexpressed in various malignancies and is correlated with aggressive phenotypes and unfavorable outcomes [6]. Tumor cells that overexpress GRN or secrete GRN-rich extracellular vesicles have been shown to drive TAMs toward an immunosuppressive M2 phenotype, thereby establishing a suppressive network within the tumor microenvironment [7, 8]. Collectively, these findings highlight the close association between GRN expression and tumor-associated macrophage (TAM) polarization and suggest that GRN may be involved in the development of the GBM tumor microenvironment and therapeutic resistance and may serve as a potential therapeutic target.

M2-polarized tumor-associated macrophages (TAMs) secrete a variety of protumor cytokines, including IL-10 and TGF-β, which significantly promote the invasiveness and therapeutic resistance of glioma, ultimately shortening the survival time of patients [9, 10]. In addition, an analysis of public datasets indicated that higher GRN expression levels are associated with a poorer prognosis, and these findings suggest that GRN may promote glioma progression by regulating TAM polarization [11, 12]. However, the specific molecular role of GRN in GBM and the underlying mechanism by which it modulates M2 polarization remain elusive. In addition, GRN is closely correlated with the initiation and progression of GBM. It can facilitate the development of temozolomide resistance by regulating DNA repair pathways and enhancing the characteristics of cancer stem cells. Therefore, GRN is considered a potential therapeutic target with considerable value [13, 14].

Sortilin (SORT1), a high-affinity cell membrane receptor and soluble protein that binds progranulin (pGRN), plays a central regulatory role in the endocytosis, lysosomal trafficking, and degradation of pGRN, serving as a key molecule governing intracellular and extracellular pGRN levels. Together, these proteins form a bidirectionally regulated functional axis whose dysfunction is closely associated with the pathogenesis and progression of neurodegenerative diseases [15]. Extracellular SORT1 binds to GRN and attenuates its biological activity via a receptor-ligand-mediated mechanism [16]. This study investigated the application of a photocrosslinked hyaluronic acid (HA)-based hydrogel (HAMA) as a local drug delivery system to treat GBM. Featuring controlled drug release and excellent biocompatibility, this system can cross the blood-brain barrier and precisely target residual tumor cells after surgery [17]. In experiments using tumor-bearing animals, SORT1-loaded HAMA microspheres markedly inhibited GBM growth, reduced the abundance of M2-type macrophages and decreased the pGRN protein level. These findings indicate that targeting GRN represents a novel and potentially effective therapeutic strategy for GBM.

Materials and methods

Cell culture

GBM cells (A172 and LN229 cell lines, purchased from Shanghai Jinyuan Biotechnology Co., Ltd., Shanghai, China) and primary human peripheral blood macrophages (purchased from Shanghai Jinyuan Biotechnology Co., Ltd., Shanghai, China) were cultured in low-glucose DMEM supplemented with 10% fetal bovine serum (FBS) and 100 U/mL penicillin. Primary human peripheral blood macrophages were positive for CD68 and MAC387, as confirmed by immunofluorescence staining, with a purity greater than 90%. To further verify their unpolarized state, flow cytometry analysis of polarization markers showed that the proportions of CD86, CD197, CD206, and CD163 positive cells were all below 5% (Figure S1), indicating that these macrophages were in a resting M0 phenotype. All the cells were cultured in a humidified incubator at 37°C with 5% CO_2. Routine subculture was performed by trypsin digestion, and only cells with a passage number not exceeding 10 were used in all the experiments. GBM cells were treated with the TGF-β receptor inhibitor LY3200882 (MCE, New Jersey, USA) at a final concentration of 10 μM, which was dissolved in DMEM prior to use.

Cell transfection

GBM cells were cultured in complete medium and seeded 24 h prior to transfection to achieve 30-50% confluence. Gene silencing was performed using a small interfering RNA (siRNA) targeting GRN (siRNA sequence: 5'-GGA CCU GUG AGA AGG AUG UCG AUU-3', purchased

from Fenghui Biotechnology Co., Ltd.). The cells were transfected with 50 nM siRNA. Briefly, 1 μL of LipofectamineTM 3000 Reagent and 1 μL of P3000™ Reagent were diluted in 50 μL of Opti-MEM™ medium (Gibco, Grand Island, NY, USA). The diluted siRNA and Lipofectamine 3000 reagents were mixed gently by pipetting and incubated at room temperature for 10-15 min to allow the formation of siRNA-lipid complexes. The resulting complexes (50 μL per well) were added to cells cultured in 24-well plates. The plates were then returned to a 37°C incubator with 5% CO_2 and cultured for 18-48 h before subsequent assays.

Wound healing assay

GBM cells were divided into siNC and siGRN groups. When the cells reached 80-90% confluence in 6-well plates, a linear scratch was created in the cell monolayer using a 10 μL pipette tip. The culture medium was replaced with DMEM containing 1% fetal bovine serum (FBS). Images were captured immediately after scratching and again at 24 h and 48 h after scratching. Wound closure at these time points was compared to evaluate differences in cell migration between the two groups.

Colony formation assay

siNC-transfected and siGRN-transfected GBM cells were seeded into 6-well plates at a density of 1×10^3 cells per well. After 2 weeks of culture with regular medium replacement, the cell colonies were fixed with methanol for 5 min and stained with 0.1% crystal violet for 5 min. The plates were then washed three times with ddH_2O. The colony-forming ability was evaluated by counting the number of stained cell colonies in 3 randomly selected microscopic fields.

Cell counting kit-8 assay

Cell proliferation was assessed using a CCK-8 assay kit (Beyotime Biotechnology, Shanghai, China). Briefly, cells were seeded in 96-well plates and cultured under routine incubation conditions. At the designated time points (0 h, 24 h, and 48 h), 10 μL of CCK-8 reagent was added to each well containing 100 μL of culture medium in accordance with the manufacturer's instructions. Following an incubation at 37°C for 2 h, the absorbance at 450 nm was detected using a microplate reader. The obtained optical density values were utilized to quantitatively evaluate cell proliferation.

Invasion assay using Matrigel-coated Transwell chambers

Cell invasion was evaluated using the Matrigel-coated Transwell chamber method. Matrigel was diluted according to the manufacturer's instructions and spread on the membrane of the upper Transwell chamber (pore size 8 μm), followed by an incubation at 37°C with 5% CO_2 for 30-60 min to allow solidification. Logarithmic-phase GBM cells were adjusted to a density of 5×10^4 cells/well and seeded into the coated upper chamber; DMEM supplemented with 1% FBS was added to the lower chamber, while equal numbers of macrophages or GBM cells were added to the lower chamber of the control group, with 3 replicate wells in each group. After 24 h of incubation, non-invading cells on the upper surface of the chamber membrane were wiped off with a sterile cotton swab. Invading cells on the lower surface were fixed with methanol for 10 min, stained with crystal violet for 10 min, rinsed with PBS, and then air-dried. The cells were observed and photographed under an inverted microscope. Five random fields of view were selected from each replicate well for cell counting, and the average number of invading cells was calculated to quantitatively evaluate the invasion of GBM cells.

Immunofluorescence staining in Transwell co-culture system

A Transwell co-culture system was established to evaluate TGF-β/Smad signaling activation in GBM cells. Macrophages were seeded in the upper chamber, while GBM cells were plated in the lower chamber. Four experimental groups were set up with different treatments applied to GBM cells: IgG (control), IgG + LY3200882 (LY), anti-TGF-β1 neutralizing antibody, and IgG + recombinant TGF-β1.

After 3 days of co-culture, GBM cells in the lower chamber were collected and fixed with 4% paraformaldehyde for 15 min at room temperature, followed by permeabilization with 0.1% Triton X-100 for 10 min. Cells were then blocked with 5% bovine serum albumin (BSA) for 1 h at room temperature and incubated overnight at 4°C with primary antibody against

phospho-Smad2 (p-Smad2; Proteintech, Cat# 80427-2-RR) at a dilution of 1:400.

After washing with PBS, cells were incubated with an appropriate fluorescent secondary antibody for 1 h at room temperature in the dark. Nuclei were counterstained with DAPI. Fluorescence images were captured using a fluorescence microscope, and the expression of p-Smad2 was analyzed.

Real-time quantitative PCR

Total RNA was isolated and purified using a RNeasy Mini Kit (Qiagen, Germantown, MD, USA) according to the manufacturer's instructions. The cDNA primers used were obtained from Dalian Ruizhong Biotechnology Co., Ltd., and an RT-PCR analysis was subsequently performed. We normalized the cycle threshold (Ct) value of the gene of interest to the Ct value of GAPDH in the same sample and calculated the relative expression using the $2^{-\Delta\Delta Ct}$ method.

IL-6 F-ACTCACCTCTTCAGAACGAATTG, R-CCATCTTTGGAAGGTTCAGGTTG; TGF-β1 F-CTGCTGACCCCCACTGATAC, R-TGACCCGTTGATGTCCACTT; TNF-α F-CCTCTCTCTAATCAGCCCTCTG, R-GAGGACCTGGGAGTAGATGAG; IL-10 F-GACTTTAAGGGTTACCTGGGTTG, R-TCACATGCGCCTTGATGTCTG; TWIST1 F-GGAGTCCGCAGTCTTACGAG, R-TCTGGAGGACCTGGTAGAGG; SNAI2 F-TGTTGCAGTGAGGGCAAGAA, R-GACCCTGGTTGCTTCAAGGA; MMP2 F-TTGATGGCATCGCTCAGATC, R-TTGTCACGTGGCGTCACAGT; MMP9 F-GCAAGCTGGACTCGGTCTTT, R-TGGCGCCCAGAGAAGAAG.

Preparation and physicochemical characterization of the hydrogel microspheres

HAMA microspheres (molecular weight 400 kDa) were prepared as follows: HAMA was dissolved in a 1%-5% PBS solution containing 0.2% photoinitiator (LAP) and 100 pg/mL SORT1. Microspheres were prepared using the microfluidic focusing method. The oil phase was composed of HFE-7500 and 2% PEG-PFPE EA surfactant. By regulating the flow rates (aqueous phase: 10-50 μL/h; oil phase: 500-2000 μL/h), droplets with a particle size of less than 100 μm were generated, which were then polymerized under 365 nm ultraviolet light. The residual oil phase and unreacted reagents were removed by washing to obtain HAMA hydrogel microspheres.

The particle size of the microspheres was analyzed. After the microsphere suspension was diluted, it was dropped onto a glass slide and covered with a coverslip. After an incubation, the samples were observed under an optical microscope. No less than 3 fields of view were randomly selected, and no fewer than 50 microspheres in each field of view were counted. The micrographs were analyzed using ImageJ software to identify the microspheres and measure their equivalent circular diameter. The measured data were imported into Origin software to construct a particle size distribution histogram, and Gaussian curve fitting was performed to visualize the particle size distribution of the microspheres in the histogram and fitted curve.

For the microsphere degradation experiment, the hydrogel microspheres were placed in 1 mL of a PBS solution containing 1,000 U of alginate lyase and cultured with shaking at 37°C and 80 rpm for 48 hours, after which the alginate lyase solution was replaced regularly. After culture, the remaining mass of the microspheres was measured, the treatment was standardized such that the initial mass was used as the reference, and the degradation characteristics of the microspheres were analyzed.

Xenograft models

We divided the A172 cells into three groups: the untreated control group, the HAMA microsphere group, and the HAMA@SORT1 microsphere group, with four samples in each group. A total of 2×10^6 cells were subcutaneously injected into 5-week-old BALB/c nude mice. One week later, the mice in each group received an intratumoral injection of 100 μL of HAMA or HAMA@SORT1 microsphere suspension. Starting on the 5th day after treatment, the length and width of the tumors were measured and recorded every 5 days. The tumor volume was calculated using the following formula: length × width × width × 0.5. On the 20th day, the tumors were removed and weighed. At the end of the experiment, the mice were fully anesthetized with inhalation anesthesia and then euthanized by cervical dislocation, ensuring a painless death in accordance with animal ethics guidelines. All procedures were approved by the Institutional Animal Care and Use Committee (Approval No. D2023-034).

Immunohistochemical staining

Paraffin-embedded GBM tumor-bearing tissues (Subcutaneous xenograft tumor tissues of A172 cells in nude mice) were serially sectioned at 4 μm thickness and mounted on poly-L-lysine-coated glass slides. After the samples were dewaxed in xylene and rehydrated through a graded ethanol series, antigen retrieval was performed in 0.01 mol/L sodium citrate buffer (pH 6.0) at 95°C for 15 min using a pressure cooker. Endogenous peroxidase activity was blocked with 3% H_2O_2 for 10 min at room temperature, followed by an incubation with 5% bovine serum albumin (BSA) for 30 min to minimize nonspecific binding. The sections were then incubated overnight at 4°C in a humidified chamber with the following primary antibodies: pGRN (1:500, Abcam, ab208777), TGF-β1 (1:500, Abcam, ab315255), and CD163 (1:500, Abcam, ab213612). After three washes with PBS, the corresponding HRP-conjugated secondary antibody (1:500) was applied to the sections and incubated for 1 h at room temperature. The color was developed using a DAB chromogenic kit (Beijing Zhong Shan-Golden Bridge Biological Technology Co., Ltd.) for 3 min. The sections were counterstained with hematoxylin for 30 s, dehydrated through graded ethanol solutions, cleared in xylene, and mounted with neutral resin. Images were captured at 20× magnification.

Bioinformatics analysis

Gene expression matrices and clinical data were retrieved from the GEO database (GSE90598), and TPM-format transcriptomic data (log2(TPM+1)) for GBM tumor tissues were obtained from TCGA. Quality control was performed on both datasets to remove missing values and outliers. The differential expression analysis was conducted using the R package limma (v3.60.6), with screening criteria set at adjusted p value < 0.05 and |logFC| > 1. Genes with logFC > 1 were defined as upregulated, and those with logFC < -1 were defined as downregulated. Differentially expressed genes (DEGs) were visualized in volcano plots generated with ggplot2 (v3.5.1). The intersections of upregulated and downregulated DEGs from the GEO dataset and prognosis-related genes from TCGA (identified via Cox regression analysis) were calculated and visualized using VennDiagram (v1.7.3) and ggVennDiagram (v1.5.2). For the GRN-based grouping, the surv_cutpoint function from the survminer package (v0.5.0) was used to determine the optimal cutoff of GRN expression, dividing the samples into high- and low-expression groups. Differences in GRN expression between groups were compared using the Wilcoxon rank-sum test ($P < 0.05$) and visualized in bar plots generated by ggplot2 (v3.5.1). Kaplan-Meier survival analysis was performed using the survival (v3.6.4) and survminer (v0.5.0) packages, and differences in survival were assessed using the log-rank test. Immune cell infiltration in TCGA-GBM datasets was analyzed using CIBERSORT (v0.1.0) to estimate the relative abundances of 22 immune cell types, while the ESTIMATE algorithm (v1.0.13) was used to calculate the immune score, stromal score, and total ESTIMATE score. Differences in immune cell infiltration and TME scores between the high- and low-GRN expression groups were evaluated using the Wilcoxon rank-sum test and visualized in stacked bar plots and statistical plots generated using ggplot2 (v3.5.1).

Statistical analysis

All statistical analyses were performed using SPSS 25.0 software (IBM, Armonk, NY, USA) and R software (version 4.5.3, http://www.r-project.org). Continuous variables are expressed as the mean ± standard deviation (SD). Comparisons between two groups were performed using independent-sample t-tests for normally distributed data, and the Mann-Whitney U test for non-normally distributed data. One-way analysis of variance (ANOVA) followed by post hoc tests was used for comparisons among three or more groups. For in vitro experiments, each assay was performed in at least three independent biological replicates to ensure reproducibility. Kaplan-Meier curves were plotted to estimate overall survival (OS) and progression-free survival (PFS), and differences between groups were compared using the log-rank test. Univariate and multivariate Cox proportional hazards regression models were applied to identify independent prognostic factors and calculate hazard ratios (HR) with 95% confidence intervals (95% CI). Spearman's correlation analysis was used to evaluate the monotonic relationship between non-normally distributed quantitative variables, including

GRN and CD163 expression. All statistical tests were two-sided, and a *P*-value < 0.05 was considered statistically significant.

Results

GRN as a poor prognostic factor and potential therapeutic target in GBM

Gene expression data (GSE90598) were downloaded from the GEO database and subjected to quality control to ensure the integrity of the data. Paired tumor and adjacent nontumor tissues were analyzed for differential gene expression using the R package limma (v3.60.6). Genes with an adjusted *p* value < 0.05 and logFC > 1 were classified as upregulated, whereas those with an adjusted *p* value < 0.05 and logFC < -1 were classified as downregulated. Volcano plots of the differentially expressed genes (DEGs) were created using the ggplot2 package (v3.5.1). A total of 816 upregulated and 1,267 downregulated genes were identified (**Figure 1A**). Among these genes, 567 upregulated and 947 downregulated genes matched the TPM data from TCGA database. Furthermore, an analysis of the intersections of the DEGs with 588 prognosis-associated genes identified via Cox regression analysis of TCGA-GBM data revealed 22 upregulated and 50 downregulated genes with significant prognostic relevance (**Figure 1B**). Among them, GRN was selected as one of the 22 significantly upregulated genes associated with prognosis in the TCGA-GBM cohort and was prioritized for further study because of its known role in promoting tumor progression, inflammation, and cell proliferation in various cancers. TCGA-GBM data were used to analyze the relationship between GRN expression and patient survival as an indicator of its clinical value, with a focus on its potential as a prognostic biomarker. GBM STAR count data and clinical information were obtained from the TCGA database. The data in TPM format were extracted and normalized using log2(TPM+1) transformation, and 153 samples with both RNA-seq and clinical data were retained. The log-rank test and univariate Cox regression analyses revealed that overall survival and progression-free survival were significantly lower in the high-GRN expression group than in the low-GRN expression group (*p* value and HR with 95% CI) (**Figure 1C**, **1D**).

GRN expression modulates immune cell infiltration and the tumor microenvironment in GBM

We analyzed tumor samples from the TCGA dataset with available survival information to investigate the relationship between GRN expression and immune cell infiltration in GBM. Using the CIBERSORT algorithm, we evaluated the relative infiltration levels of 22 immune cell types in the high- and low-GRN expression groups. The results revealed significant differences in the levels of immune cell infiltration between the two groups (**Figure 1E**). Specifically, we quantified the proportions of immune cell types, including B cells (naive and memory), plasma cells, T cells ($CD8^+$, $CD4^+$ naive, $CD4^+$ memory resting, $CD4^+$ memory activated, follicular helper, regulatory, and gamma delta T cells), NK cells (resting and activated), monocytes, macrophages (M0, M1, and M2), dendritic cells (resting and activated), mast cells (resting and activated), eosinophils, and neutrophils. A stacked bar plot generated using ggplot2 visually illustrates the distributions of these immune cells, highlighting distinct immune profiles between the high- and low-GRN-expressing groups (**Figure 1E**). Further analysis using the ESTIMATE algorithm revealed highly significant differences in the immune, stromal, and ESTIMATE scores between the high- and low-GRN-expressing groups ($P < 0.001$ for all scores) (**Figure 1E**). These findings indicate a strong association between GRN expression levels and tumor microenvironment (TME) characteristics in GBM. We performed Wilcoxon rank-sum tests to compare the levels of infiltration of specific types of immune cells between the two groups and identify the cell type contributing to the differences in these scores. Significant differences were observed for several immune cell types ($P < 0.05$), including plasma cells, naive $CD4^+$ T cells, resting $CD4^+$ memory T cells, activated NK cells, M2 macrophages, and resting dendritic cells (**Figures 1F**, **1G**, S2). Spearman's correlation analysis revealed a significant positive correlation between GRN expression and CD163 expression. These observations were further validated by analyzing mRNA expression profiles derived from tissues samples from 153 GBM patients in The Cancer Genome Atlas (TCGA) database, which consistently revealed a strong positive correlation between GRN and CD163 expres-

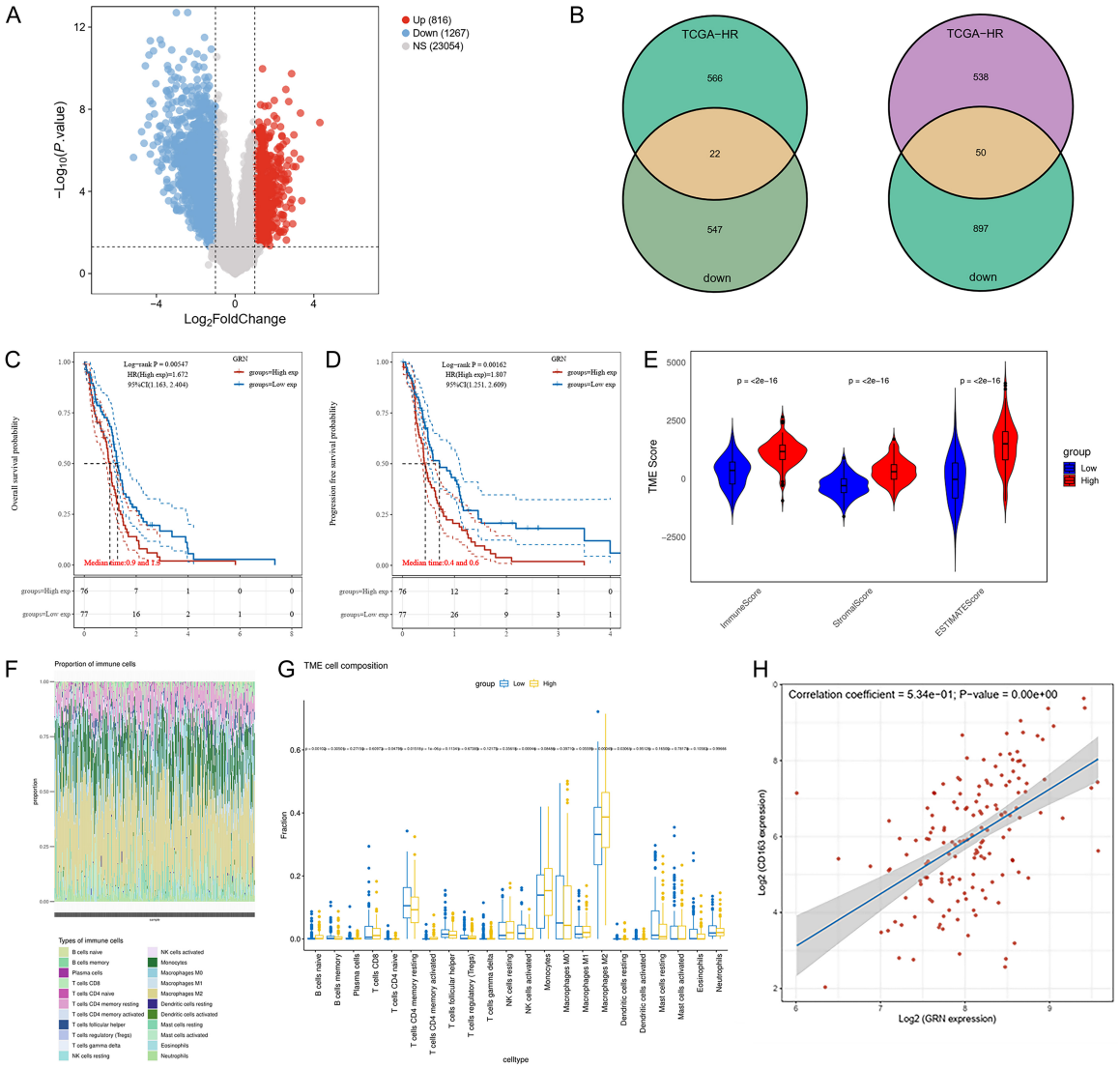

Figure 1. GRN expression and its prognostic and immunological implications in GBM. (A) Volcano plot depicting differentially expressed genes (DEGs) from the GSE90598 dataset, which was analyzed using limma (v3.60.6). Upregulated genes (adjusted p value < 0.05, logFC > 1) and downregulated genes (adjusted p value < 0.05, logFC < -1) are shown, with 816 upregulated and 1,267 downregulated genes identified. (B) Venn diagram illustrating the intersections of DEGs with 588 prognosis-associated genes in TCGA-GBM data; 22 upregulated and 50 downregulated genes with prognostic relevance were identified, and GRN was among the upregulated genes. (C, D) Kaplan-Meier survival curves and univariate Cox regression analysis of TCGA-GBM data (n = 153) showing significantly lower overall survival (C) and progression-free survival (D) rates in the high-GRN expression group than in the low-GRN expression group (log-rank p value and HR with 95% CI). (E) Stacked bar plot generated with ggplot2 displaying the relative infiltration of 22 immune cell types in TCGA-GBM cohort stratified by high and low GRN expression, which was analyzed using CIBERSORT. Significant differences in immune, stromal, and ESTIMATE scores between groups are shown (P < 0.001). (F, G) Box plots illustrating significant differences in the infiltration levels of specific immune cell types (plasma cells, naive CD4$^+$ T cells, resting CD4$^+$ T cells, activated NK cells, M2 macrophages, and resting dendritic cells) between the high- and low-GRN-expressing groups in TCGA-GBM cohort, as determined using Wilcoxon rank-sum tests (P < 0.05). (H) Spearman's correlation analysis of the GRN and CD163 mRNA expression data from the tissues from 153 GBM patients in TCGA database revealed a consistent positive correlation (R = 0.53, P < 0.001).

sion (R = 0.53, P < 0.001) (**Figure 1H**). Collectively, these results indicate that the GRN expression level is significantly associated with specific immune cell infiltration patterns and TME characteristics in GBM. The significant differences in certain immune cell populations

suggest their potential roles in tumor progression in the presence of varying GRN expression levels. These findings provide a foundation for further investigations into TME regulation and potential immunotherapeutic targets in GBM.

Effects of GRN expression on the phenotypes of GBM cells

The level of the GRN protein in the cell culture supernatant was quantified using enzyme-linked immunosorbent assay (ELISA) to confirm the efficiency of GRN knockdown. Compared with the transfection of the negative control (siNC) GRN expression was significantly reduced in A172 cells transfected with the GRN-specific siRNA (**Figure 2A**), indicating the effective knockdown of GRN in this cell line. A similar reduction was observed in LN229 cells (Figure S3A). Cell proliferation was further assessed using the CCK-8 assay. Compared with the transfection of siNC, GRN knockdown using an siRNA significantly suppressed the proliferation of A172 cells (**Figure 2B**). Consistent results were obtained in LN229 cells (Figure S3B), suggesting that GRN plays a critical role in promoting GBM cell proliferation. Cell migration was evaluated by performing a wound-healing assay, with wound closure recorded at 0, 24, and 48 h. Compared with the control treatment, GRN knockdown significantly inhibited the migration of A172 cells, as evidenced by slower wound closure and markedly fewer cells within the wound area (**Figure 2C-E**). Similar trends were observed in LN229 cells (Figure S3C, S3D). In addition, a single-cell colony formation assay was performed to detect tumorigenicity in vitro. Compared with control cells, siGRN-transfected A172 cells formed significantly fewer and smaller colonies (**Figure 2F-H**). The same pattern was observed in LN229 cells (Figure S3E, S3F), demonstrating that GRN silencing substantially impaired the clonogenic ability of GBM cells. Collectively, these results indicate that GRN promotes proliferation, migration, and tumorigenicity in GBM cells, supporting its key function in driving glioblastoma malignancy.

GRN mediates intercellular communication between GBM cells and macrophages

Macrophages were cocultured with siNC-GBM or siGRN-GBM cells to investigate the regulatory effect of GBM cell-derived GRN on macrophage polarization. Flow cytometry was used to detect the expression of the macrophage polarization markers CD206 (M2) and CD197 (M1). Compared with that in the siNC-GBM group, the proportion of $CD206^+$ M2-like macrophages was significantly decreased, while the proportion of $CD197^+$ M1-like macrophages was markedly increased in the siGRN-GBM coculture system (**Figure 3A-E**). These findings were further validated using another set of classical markers, CD163 (M2) and CD86 (M1), which yielded consistent results: GRN knockdown in GBM cells significantly promoted macrophage polarization toward the M1 phenotype (Figure S4A-D). Collectively, these data indicate that GRN secreted by GBM cells drives macrophage polarization toward the immunosuppressive M2 phenotype, whereas GRN silencing shifts polarization toward the proinflammatory M1 phenotype, which may inhibit GBM progression.

Four coculture systems were established in Transwell invasion assays to evaluate the effect of GBM-derived GRN on tumor cell invasion: a control group with siNC-GBM cells in both the upper and lower chambers (siNC-GBM/siNC-GBM); a group with siGRN-GBM cells in both chambers (siGRN-GBM/siGRN-GBM), and two additional groups in which siNC-GBM or siGRN-GBM cells were seeded in the upper chamber and human macrophages were plated in the lower chamber (siNC-GBM/Mφ and siGRN-GBM/Mφ). This design allowed the cell-autonomous effects of GRN knockdown and the effects tumor cell-macrophage interactions to be differentiated, thereby clarifying the role of GRN within the tumor microenvironment.

Transwell invasion assays revealed that the number of invading cells was significantly reduced in the siGRN-GBM/siGRN-GBM group compared with the siNC-GBM/siNC-GBM control group (**Figure 3F**, **3G**, **3J**), indicating that GRN knockdown attenuated the intrinsic invasive capacity of GBM cells. Notably, the siNC-GBM/Mφ coculture group exhibited a significantly greater number of invading cells than the siNC-GBM/siNC-GBM group (**Figure 3H**), confirming that macrophages promote GBM cell invasion. Importantly, this pro-invasive effect was markedly attenuated in the siGRN-GBM/Mφ group compared with that in the siNC-GBM/Mφ group (**Figure 3H-J**), suggesting that the macrophage-mediated promotion of GBM invasion depends on GRN expression and secre-

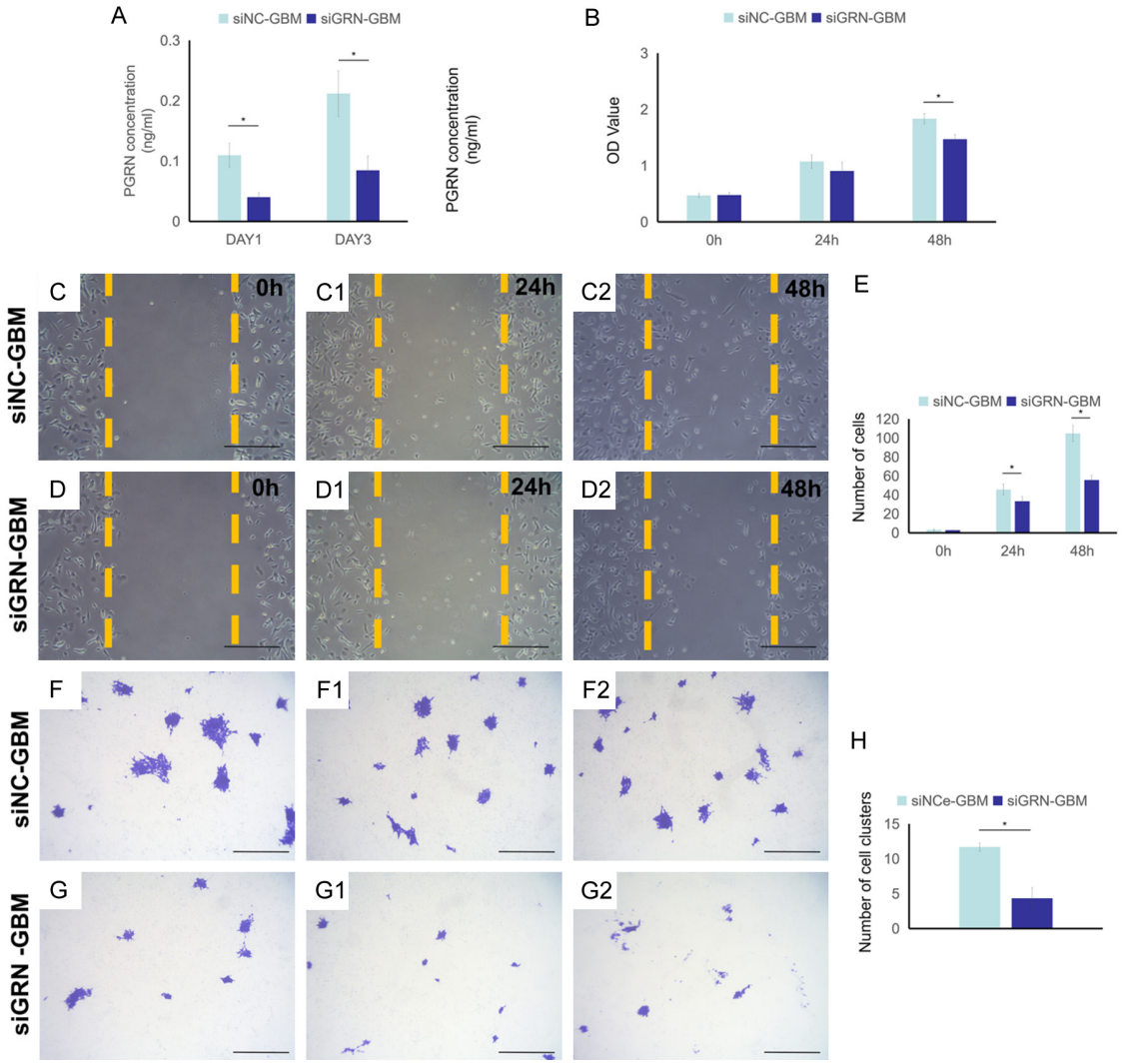

Figure 2. GRN knockdown suppresses the malignant phenotypes of GBM cells. A. The level of GRN secreted by siNC- and siGRN-transfected GBM cells was quantified using ELISA. B. The effect of GRN knockdown on GBM cell proliferation was assessed using a CCK-8 assay. C-E. Wound healing assays were performed at 0, 24, and 48 h to evaluate the effect of GRN knockdown on the migration of GBM cells. The number of cells migrating into the area delineated by yellow dashed lines was quantified. F-H. The effects of GRN knockdown on the clonogenic and tumorigenic potential of GBM cells were determined using single-cell colony formation assays. Scale bar: 250 μm; *P < 0.05.

tion. Taken together, these findings reveal that GRN facilitates tumor cell invasion by mediating crosstalk between GBM cells and macrophages, thereby playing a pivotal role in intercellular communication and immune microenvironment remodeling within the tumor niche.

A GRN-TGF-β feedback loop is involved in the intercellular communication between GBM cells and macrophages

RT-PCR results showed that, compared with the control co-culture group (siNC-GBM/Mφ), co-culture with GRN-knockdown GBM cells (siGRN-GBM/Mφ) markedly suppressed the mRNA expression of IL-10 and TGF-β1 in macrophages, while significantly upregulating the expression of IL-6 and TNF-α (**Figure 4A**). Consistent with these findings, ELISA further confirmed that the protein level of TGF-β1 was notably decreased in the supernatant of the siGRN-GBM/Mφ co-culture system (**Figure 4B**). Notably, the synchronous downregulation of macrophage-derived TGF-β1, a pro-tumor cytokine, suggests the existence of a potential GRN-TGF-β feedback loop between GBM cells

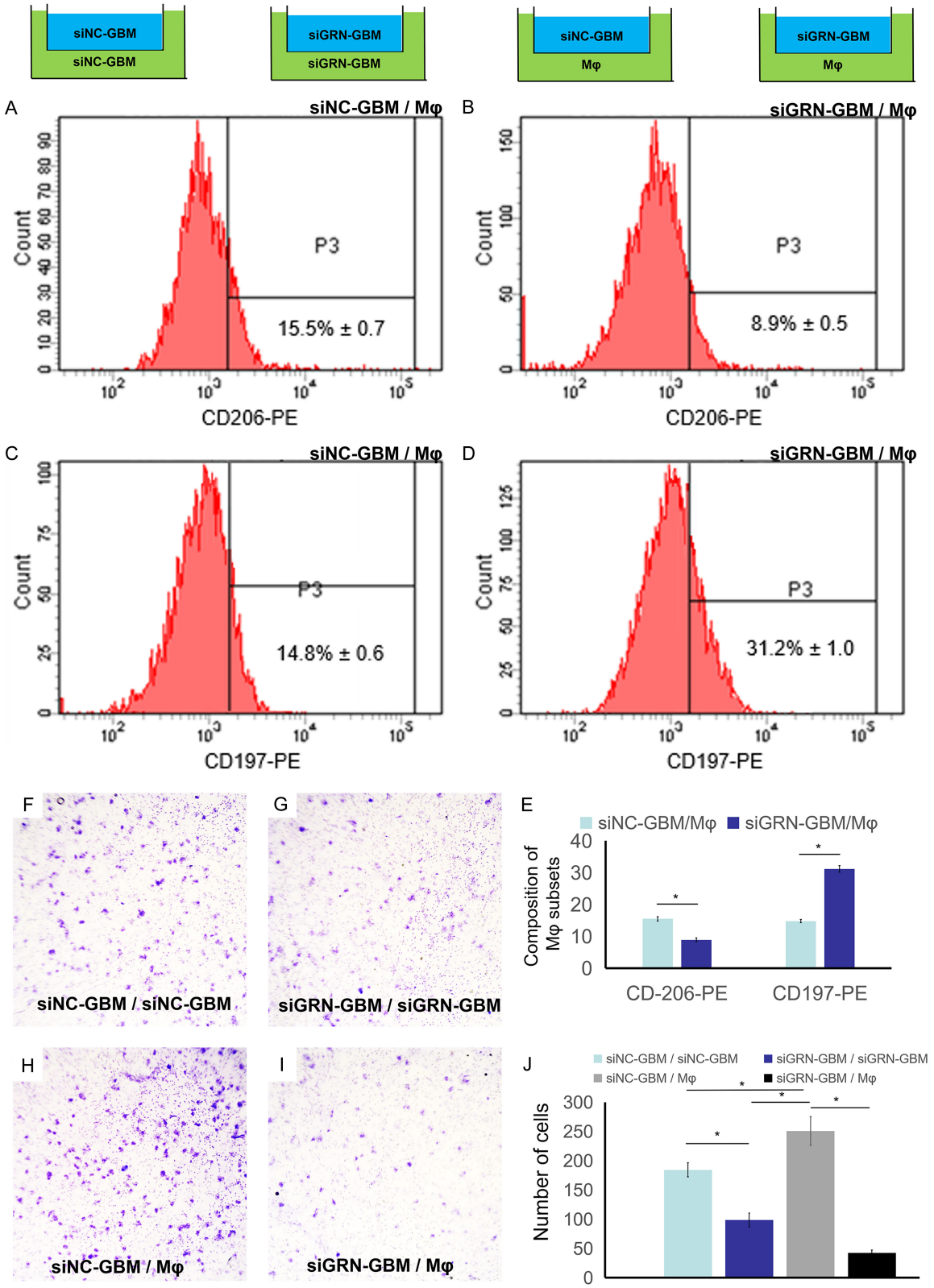

Figure 3. GRN-mediated immune interactions between GBM cells and macrophages. A-E. Flow cytometry analysis revealed an increase in the number of M1 macrophages ($CD197^+$) and a decrease in the number of M2 macrophages ($CD206^+$) in the coculture with siGRN-GBM cells. F-J. A Transwell coculture system was used to compare the invasive capacity of GBM cells under different conditions, and the number of cells migrating through the basement membrane was quantified. Scale bar: 250 μm; *P < 0.05.

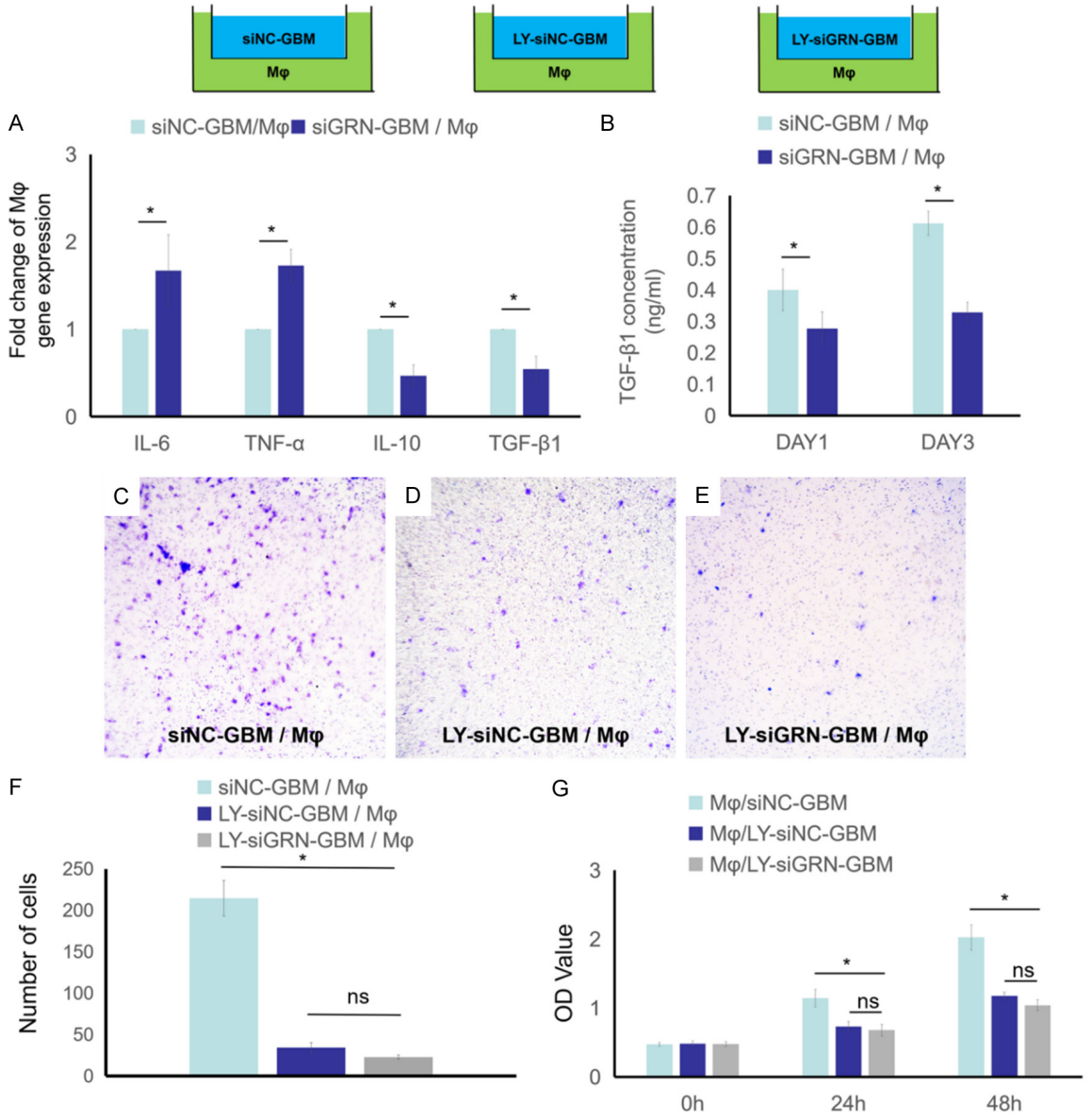

Figure 4. GRN affects GBM cell invasion and proliferation by regulating the macrophage secretory profile and TGF-β signaling. A. qPCR analysis of inflammation-related factor expression in macrophages under coculture conditions. B. ELISA of TGF-β1 levels in the coculture system. C-E. Transwell invasion assay for evaluating the invasive capacity of GBM cells under different treatment conditions. F. Quantitative analysis of the number of invaded cells in Transwell assays. G. CCK-8 assay of the proliferation of GBM cells in response to different treatments. Scale bar: 250 μm; *P < 0.05.

and macrophages. Specifically, GBM-secreted pGRN induces M2 polarization of macrophages, while M2-polarized macrophages in turn release TGF-β1 to promote the proliferation and migration of GBM cells. Three noncontact coculture systems were established to test this hypothesis: siNC-GBM/Mφ, LY+siNC-GBM/Mφ (where LY3200882, a selective TGF-β receptor I inhibitor, was added), and LY+siGRN-GBM/Mφ. Transwell invasion assays showed that LY3200882 substantially attenuated the macrophage-induced increase in the invasion of siNC-GBM cells. Furthermore, no significant difference in the invasive capacity was observed between the LY+siGRN-GBM and LY+siNC-GBM groups (**Figure 4C-E**), supporting the role of TGF-β signaling in mediating GBM-macrophage crosstalk. Cell proliferation assays further dem-

onstrated that the growth rates of both the LY+siNC-GBM and LY+siGRN-GBM groups were significantly lower than those of the untreated siNC-GBM group (**Figure 4G**). Collectively, these results indicate that reducing GRN expression in GBM cells suppresses the M2 polarization of macrophages and inhibits paracrine TGF-β signaling, thereby restricting GBM progression.

Different coculture treatment systems were established to investigate the regulatory role of macrophage-derived TGF-β1 in the biological behavior of GBM cells and the TGF-β/Smad signaling pathway. First, macrophages were seeded in the upper chamber, and the proliferative capacity of the GBM cells in the lower chamber was assessed using a CCK-8 assay (**Figure 5A**). Compared with Mφ/IgG+GBM treatment, exogenous TGF-β1 treatment (Mφ/IgG+TGF-β1+GBM) significantly promoted GBM cell proliferation. In contrast, the addition of the TGF-β receptor inhibitor LY3200882 (Mφ/IgG+LY+GBM) or a TGF-β1 neutralizing antibody (Mφ/Anti-TGF-β1+GBM) partially or completely reversed this pro-proliferative effect, indicating that macrophages promote GBM cell proliferation via the paracrine secretion of TGF-β1. Next, immunofluorescence staining was performed to detect the level of phosphorylated Smad2 (p-Smad2) in GBM cells from the lower chamber (**Figure 5B-E**). Under basal coculture conditions (Mφ/IgG+GBM), GBM cells exhibited moderate p-Smad2 signals. Exogenous TGF-β1 treatment markedly increased the p-Smad2 fluorescence intensity, whereas treatment with LY3200882 or the anti-TGF-β1 neutralizing antibody significantly reduced p-Smad2 levels, indicating that the TGF-β/Smad signaling pathway was effectively activated. Furthermore, qPCR was performed to quantify the expression of genes downstream of the TGF-β/Smad pathway (**Figure 5F**). Compared with the control treatment, treatment with TGF-β1 significantly increased the mRNA levels of TWIST1, SNAI2, MMP2, and MMP9, whereas treatment with LY3200882 or anti-TGF-β1 markedly suppressed their expression. These findings suggest that the TGF-β/Smad signaling pathway promotes the epithelial-mesenchymal transition (EMT) and extracellular matrix degradation in GBM cells. Taken together, these findings suggest that macrophages activate the TGF-β/Smad signaling pathway in GBM cells through TGF-β1 secretion, thereby upregulating the expression of proliferation- and invasion-related genes and playing a critical role in promoting the malignant progression of GBM.

Therapeutic effect of SORT1-loaded HAMA microspheres targeting PGRN in glioblastoma xenograft models

GBM is a highly aggressive type of brain tumor, with a recurrence rate of nearly 90%, even after surgery, radiotherapy, and chemotherapy, and the median overall survival is only 15-20 months. Residual invasive tumor cells and limited drug penetration across the blood-brain barrier remain major therapeutic challenges. Progranulin (PGRN) promotes GBM progression and represents a potential therapeutic target. Sortilin 1 (SORT1) is a transmembrane receptor protein that can also be cleaved to generate a soluble form that is present in the extracellular space and tissue fluid. SORT1 captures extracellular PGRN via receptor-ligand binding and mediates its endocytosis and subsequent lysosomal degradation, thereby negatively regulating extracellular PGRN levels and inhibiting its biological activity. Accordingly, in this study, we fabricated SORT1-loaded HAMA hydrogel microspheres using microfluidic technology to evaluate the therapeutic efficacy of the local targeting of PGRN in GBM.

Initially, microscopic imaging confirmed that the prepared HAMA@SORT1 hydrogel microspheres were homogeneously dispersed and had a regular morphology and a well-defined spherical structure (**Figure 6A**). An analysis of the particle size distribution of the HAMA@SORT1 hydrogel microspheres revealed a concentrated size profile, with diameters predominantly ranging from 70 to 90 μm, indicating favorable uniformity (**Figure 6B**). In a degradation system containing hyaluronidase (10 U/mL), the microspheres degraded gradually over time and were almost completely degraded within approximately 6 days, indicating favorable biodegradability (**Figure 6C**). An analysis of drug release kinetics showed that HAMA@SORT1 microspheres exhibited sustained and stable release characteristics in both PBS and PBS supplemented with 10 U/mL hyaluronidase, and the SORT1 concentration displayed a typical sustained-release curve over time (**Figure 6D**). HAMA or HAMA@SORT1 microspheres (100 μl/ml) were incubated in PBS

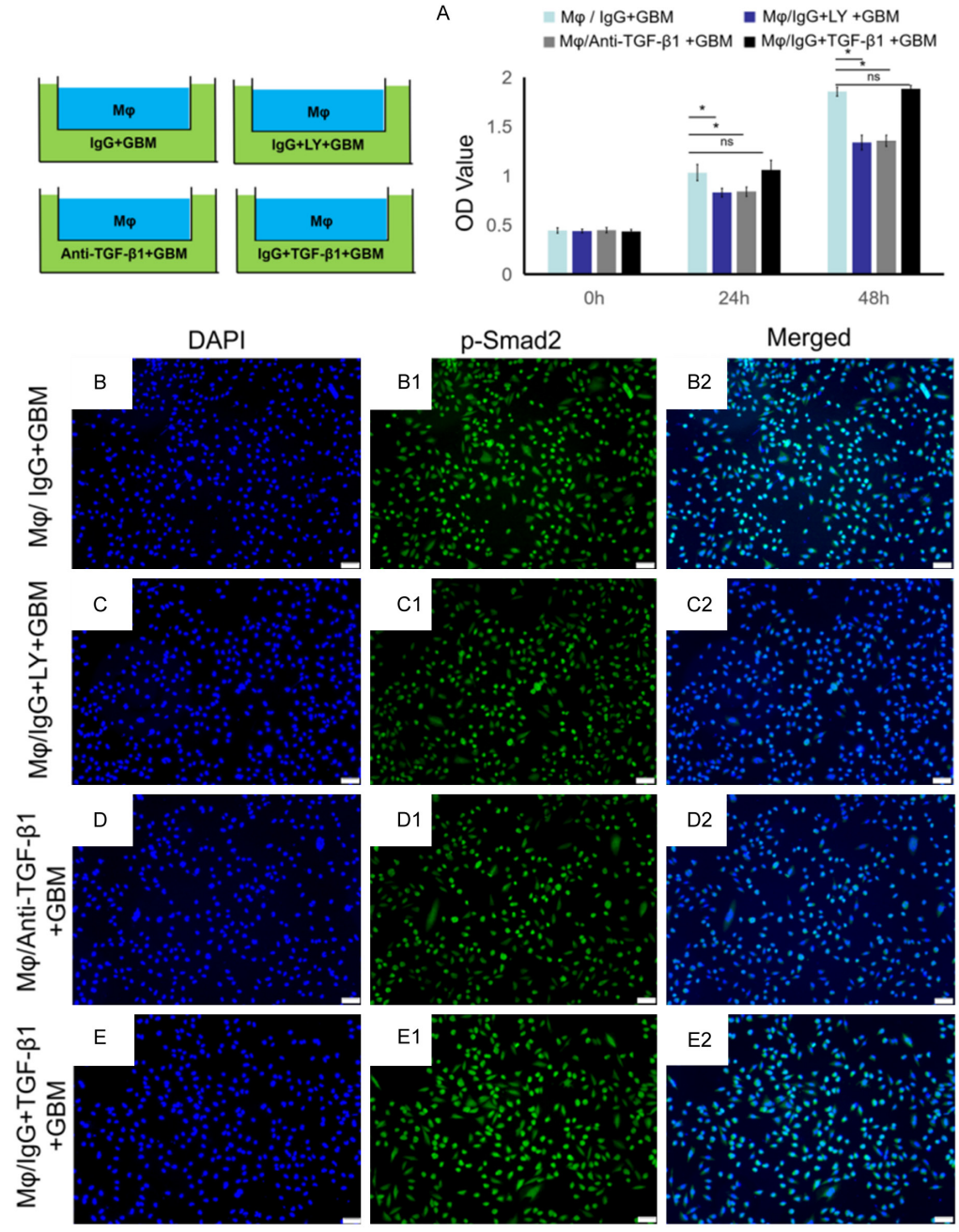
A
Mφ / IgG+GBM
Mφ/IgG+LY +GBM
Mφ/Anti-TGF-β1 +GBM
Mφ/IgG+TGF-β1 +GBM
Mφ
IgG+GBM
Mφ
IgG+LY+GBM
Mφ
Anti-TGF-β1+GBM
Mφ
IgG+TGF-β1+GBM
OD Value
0h
24h
48h
ns
DAPI
p-Smad2
Merged
B
B1
B2
Mφ/ IgG+GBM
C
C1
C2
Mφ/IgG+LY+GBM
D
D1
D2
Mφ/Anti-TGF-β1 +GBM
E
E1
E2
Mφ/IgG+TGF-β1 +GBM
F
Mφ / IgG+GBM
Mφ/IgG+LY +GBM
Mφ/Anti-TGF-β1 +GBM
Mφ/IgG+TGF-β1 +GBM
Fold change of GBM gene expression
TWIST1
SNAI2
MMP2
MMP9

Figure 5. Macrophage-derived TGF-β1 regulates the expression of tumor malignancy-related genes in GBM cells by activating the TGF-βR/Smad signaling pathway. A. A CCK-8 assay was performed to detect the proliferation of GBM cells in the lower chamber under different coculture conditions. B-E. Immunofluorescence staining was performed to determine the level of phosphorylated Smad2 (p-Smad2) in GBM cells in the lower chamber and to evaluate the activation status of the TGF-βR/Smad signaling pathway. F. qPCR was used to analyze the mRNA expression levels of tumor malignancy-related genes downstream of the TGF-β/Smad signaling pathway, including TWIST1, SNAI2, MMP2, and MMP9. Scale bar: 250 μm; *P < 0.05.

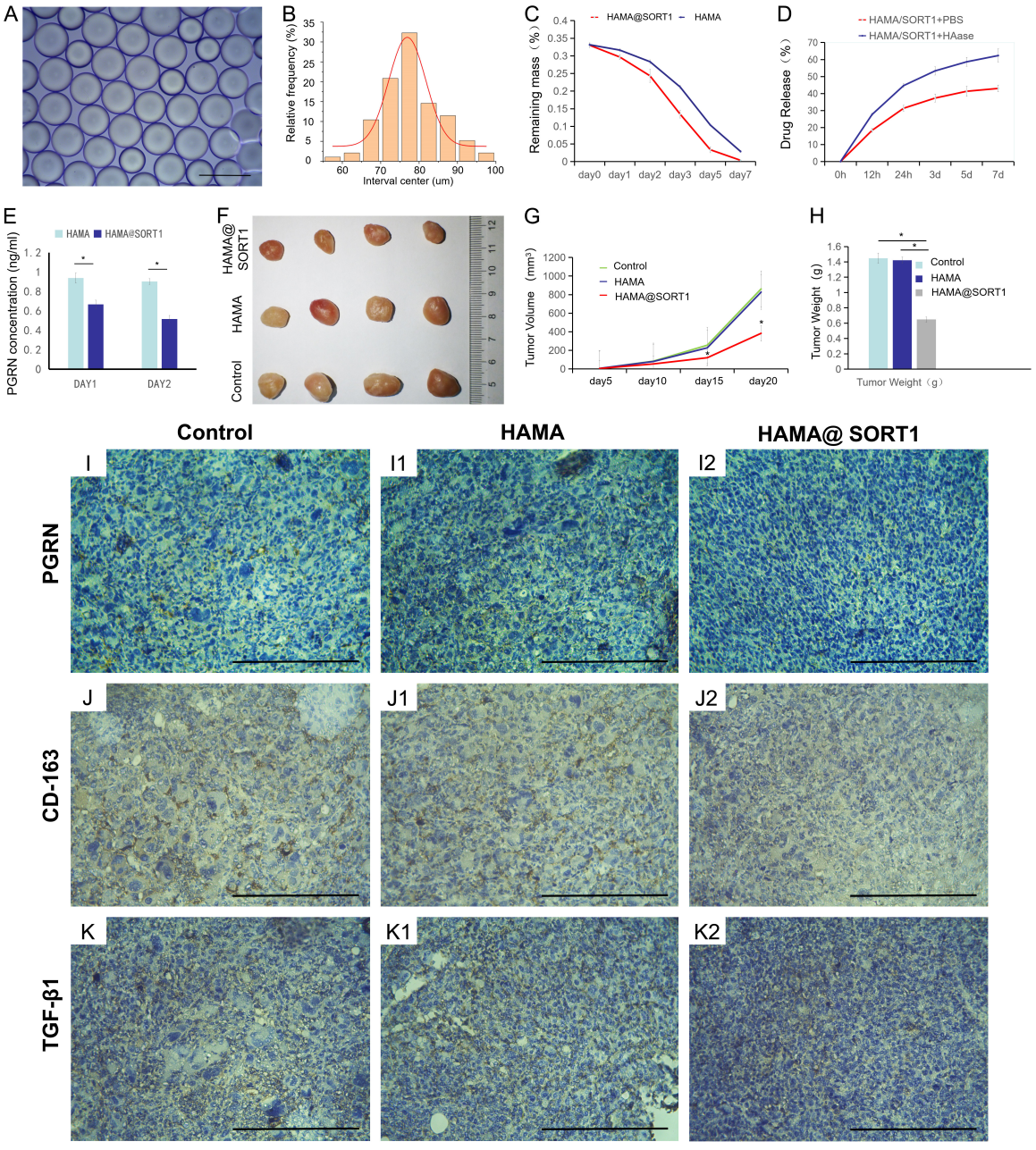

Figure 6. Therapeutic efficacy of SORT1-loaded HAMA microspheres targeting PGRN in a nude mouse model of GBM. A. Representative microscopy images of SORT1-loaded HAMA hydrogel microspheres. B. Histogram of the size distribution of the microspheres. C. Profile of the degradation of HAMA@SORT1 microspheres in the presence of hyaluronidase in vitro. D. Kinetics of SORT1 release from HAMA@SORT1 microspheres in vitro. E. Effect of HAMA@SORT1 microspheres on the PGRN concentration in vitro, as detected using ELISA. F. Representative images of subcutaneous tumors dissected from GBM xenograft model animals in the different treatment groups. G. Growth curves of tumors from Day 5 to Day 20 in the different treatment groups. H. Statistical analysis of the terminal tumor weight in each group. I-K. Immunohistochemical staining of excised xenograft tumor tissue showing the expression of PGRN, CD163 and TGF-β1. Scale bar: 150 μm; *P < 0.05.

supplemented with 1 ng/ml recombinant PGRN, and free PGRN concentrations were measured on Days 1 and 2 to assess the PGRN-capturing capacity of HAMA@SORT1 microspheres. Compared with the HAMA control, HAMA@SORT1 markedly reduced soluble PGRN levels (**Figure 6E**), indicating the specific binding and efficient clearance of PGRN by HAMA@SORT1 microspheres. The growth curve of subcutaneous xenograft tumors of A172 cells in nude mice showed that HAMA@SORT1 treatment significantly suppressed tumor progression starting on Day 15 (**Figure 6F**, **6G**). At the experimental endpoint, the tumor weights in the HAMA@SORT1 group were markedly lower than those in both the HAMA-alone group and the untreated control group (**Figure 6H**). Immunohistochemical staining revealed that HAMA@SORT1 treatment significantly reduced pGRN levels in tumor tissues compared with both no treatment and treatment with HAMA alone. Concurrently, the expression of the M2 macrophage marker CD163 and TGF-β1 was markedly decreased (**Figure 6I-K**). These results suggest that the HAMA@SORT1 system not only decreases pGRN levels but also may inhibit GBM progression by modulating the immunosuppressive tumor immune microenvironment.

Discussion

GBM is the most lethal primary brain tumor and is characterized by aggressive invasiveness, profound therapeutic resistance, and intricate interactions within the tumor microenvironment (TME) [18]. Through systematic molecular and immunological analyses, the pivotal role of GRN in driving GBM progression, particularly by modulating intrinsic tumor cell behaviors and reshaping the TME via macrophage polarization, was elucidated in the present study. Our findings demonstrate that GRN not only increases the proliferative, migratory, and invasive capacities of glioblastoma cells but also promotes M2-like macrophage polarization, thereby establishing an immunosuppressive TME. These insights provide a novel mechanistic framework for understanding glioblastoma malignancy and underscore the therapeutic potential of targeting GRN to disrupt tumor progression and improve patient outcomes.

An integrated bioinformatics analysis of the GEO and TCGA datasets revealed that GRN expression is significantly upregulated in glioblastoma (GBM) and strongly correlated with a poor clinical prognosis (**Figure 1**). These findings are consistent with those of previous reports showing that elevated GRN levels are closely associated with aggressive and invasive phenotypes across multiple human malignancies [19, 20]. The Kaplan-Meier survival analysis combined with multivariate Cox proportional hazards regression further confirmed that GBM patients with high GRN expression experienced significantly shorter overall survival (OS) and progression-free survival (PFS) than those with low GRN expression, establishing that GRN is a robust independent prognostic factor for adverse clinical outcomes (**Figure 1**). These results are consistent with those of previous reports showing that elevated GRN levels are strongly associated with a poor prognosis for multiple human malignancies, including thyroid cancer, breast cancer, and non-small cell lung cancer [21-23]. An integrated analysis of differential gene expression profiles and clinical survival data revealed that the expression of GRN was markedly upregulated in GBM tissues. High GRN expression was strongly associated with adverse clinical outcomes and retained independent prognostic significance according to the multivariate analysis. These findings establish GRN as a promising biomarker for the risk stratification and prognostic prediction of GBM.

The key findings of this study indicate that GRN contributes to the construction of the immunosuppressive tumor microenvironment (TME) in glioblastoma (GBM) by driving macrophage polarization toward the M2 phenotype. Analyses using the CIBERSORT and ESTIMATE algorithms revealed that high GRN expression was strongly associated with increased infiltration of M2 macrophages and elevated immune and stromal scores (**Figure 1F**, **1G**). Notably, GRN expression was significantly positively correlated with the expression of the M2 macrophage marker CD163 in TCGA glioblastoma cohort ($R = 0.53$, $P < 0.001$; **Figure 1H**). These results are consistent with those of previous reports showing that GRN-enriched extracellular vesicles can promote the polarization of tumor-associated macrophages (TAMs) toward an M2-like phenotype [7]. Furthermore, coculture experiments demonstrated that silencing GRN expression significantly reduced the proportion of M2-type ($CD206^+$) macrophages while con-

currently increasing the proportion of M1-type ($CD86^+$) macrophages (**Figure 3A-D**). Collectively, these findings indicate that GRN plays a central role in maintaining an immunosuppressive tumor microenvironment in GBM.

Cellular assays showed that the GRN plays a critical functional role in glioblastoma (GBM) malignancy. Stable knockdown of GRN in GBM cells (siGRN-GBM) markedly suppressed cell proliferation, migration, invasion, and the clonogenic capacity (**Figures 2**, **3F-H**), revealing that GRN actively supports the malignant phenotypes of GBM cells. These findings are consistent with previous reports documenting the association between elevated GRN expression and aggressive tumor behavior in multiple other cancer types [5, 24, 25]. In coculture systems, GBM-derived GRN potently induced macrophage polarization toward an M2-like phenotype. Conversely, GRN knockdown triggered a reciprocal shift in the expression of macrophage surface markers that was characterized by decreased expression of M2 markers ($CD206^+/CD163^+$) and increased expression of M1 markers ($CD197^+/CD86^+$) (**Figures 3A-D**, S4A-D). Moreover, macrophages significantly increased the invasive capacity of GBM cells in a strictly GRN-dependent manner; this pro-invasive effect was completely abolished following GRN silencing in tumor cells. Collectively, these results identify GRN as a key molecular mediator of intercellular communication between GBM cells and macrophages, thereby maintaining an immunosuppressive tumor microenvironment and sustaining the malignant phenotype of glioblastoma.

The present study mechanistically establishes the existence of a self-reinforcing GRN-TGF-β1 feedback loop within the glioblastoma (GBM) tumor microenvironment. GRN knockdown in GBM cells not only attenuated macrophage polarization toward the M2 phenotype (**Figure 3**) but also significantly reduced the secretion of the immunosuppressive cytokines IL-10 and TGF-β1 from M2-polarized macrophages while simultaneously increasing the levels of the pro-inflammatory cytokines IL-6 and TNF-α (**Figure 4A**, **4B**). Existing reports confirm that TGF-β activity plays an important role in mediating M2 macrophage-driven tumor growth [26-28]. Pharmacological blockade of TGF-β receptor I with LY3200882 or neutralization of TGF-β1 completely abolished the macrophage-mediated increase in GBM cell invasion and proliferation (**Figure 4C-G**), demonstrating that TGF-β1 functions as a critical downstream effector of GRN signaling. Conversely, TGF-β1 derived from macrophages or supplied exogenously robustly activated the canonical TGF-β/Smad pathway in GBM cells, as evidenced by increased Smad2 phosphorylation and the transcriptional upregulation of key genes related to the epithelial-mesenchymal transition (EMT) and extracellular matrix remodeling, including TWIST1, SNAI2, MMP2, and MMP9. These effects were fully reversed by treatment with either LY3200882 or a TGF-β1 neutralizing antibody (**Figure 5**). These findings reveal a bidirectional, self-amplifying GRN-TGF-β1 feedback loop in the GBM-macrophage microenvironment: GBM-secreted GRN drives M2 macrophage polarization, which in turn promotes paracrine TGF-β1 release that further increases tumor invasion, proliferation, and immune tolerance. This vicious cycle simultaneously amplifies immunosuppression and tumor aggressiveness, providing a mechanistic explanation for the well-documented association between elevated GRN expression and the poor prognosis of GBM patients.

Although the standard treatment regimen for GBM (surgical resection, radiotherapy, and temozolomide chemotherapy) has been well established, nearly 90% of patients still experience recurrence, with a median overall survival of less than 15-20 months [5, 9]. Following surgery, residual tumor cells frequently infiltrate the surrounding brain parenchyma, rendering complete resection extremely challenging. Moreover, the blood-brain barrier substantially restricts drug delivery, resulting in subtherapeutic drug concentrations within the tumor [17]. Local drug delivery systems can directly target residual tumor cells while bypassing the blood-brain barrier, thereby achieving controlled drug release at the tumor site and simultaneously reducing systemic exposure and toxicity. Targeting the ubiquitin-proteasome system has emerged as a promising anticancer strategy, with proteasome inhibitors such as bortezomib and carfilzomib already in clinical use; however, their application in GBM remains limited due to poor brain penetration and systemic toxicity [29]. Consequently, local delivery of agents that modulate ubiquitination-related targets, such as SORT1-loaded hydrogels, may

offer a novel approach to overcome these limitations. Based on these considerations, we designed a localized therapeutic system based on SORT1-loaded HAMA hydrogel microspheres for the treatment of GBM. HAMA is the methacrylate derivative of hyaluronic acid (HA) and can be photocrosslinked. It exhibits excellent biocompatibility, biodegradability, and stable drug release properties. Importantly, the HA backbone interacts with the highly expressed CD44 receptors on macrophages, thereby promoting receptor-mediated internalization and subsequent lysosomal degradation [30]. SORT1 specifically recognizes and binds extracellular progranulin (PGRN) in the tumor microenvironment. Through this receptor-ligand interaction, progranulin activity is inhibited, followed by endocytosis and lysosomal degradation [15, 16]. Physicochemical characterization demonstrated that the SORT1@HAMA microspheres had a particle size of 70-90 μm and underwent complete degradation within 6 days in the presence of hyaluronidase (**Figure 5A-C**). The microspheres also displayed favorable sustained-release kinetics of SORT1 and potent PGRN clearance capacity (**Figure 6A-E**). In the subcutaneous xenograft tumor model of A172 cells in nude mice, HAMA@SORT1 microspheres significantly suppressed the growth of xenograft tumors (**Figure 6F-H**). In addition, immunohistochemical staining of GBM tumor tissues revealed markedly reduced the expression of PGRN, CD163, and TGF-β1 (**Figure 6I-K**). These in vivo findings corroborate the functional role of the GRN-TGF-β1 signaling loop in GBM tissues and highlight the therapeutic potential of PGRN-targeted strategies. Furthermore, the HAMA hydrogel microsphere-based local drug delivery system represents a novel approach for clinical use.

Although this study has demonstrated the therapeutic potential of SORT1@HAMA hydrogel microspheres in suppressing GBM tumor growth and modulating the PGRN-TGF-β1 axis, several limitations remain, particularly the inability to fully recapitulate the clinical scenario of in situ microsphere implantation following GBM resection. The in vivo efficacy data presented herein were obtained exclusively from a subcutaneous A172 xenograft model using intratumoral injection of the microspheres. This model lacks critical features of the clinical setting, including the intracranial microenvironment, the surgical resection cavity, and the residual infiltrative tumor cells that drive tumor recurrence. Therefore, future studies employing intracranial orthotopic GBM models and postoperative residual tumor models will be essential to further evaluate the translational potential of this local delivery system.

Conclusion

In conclusion, this study identifies GRN as a central driver of GBM progression. By promoting M2 macrophage polarization and establishing a TGF-β1 signaling feedback loop, GRN enhances the malignant phenotypes of tumor cells while orchestrating the formation of an immunosuppressive tumor microenvironment. These mechanistic insights provide a compelling rationale for the therapeutic targeting of GRN in GBM. We engineered a locally injectable SORT1-loaded HAMA hydrogel microsphere system (SORT1@HAMA) to establish a GRN-targeted adjuvant therapeutic strategy for GBM. In the nude mouse xenograft tumor model of GBM, SORT1@HAMA resulted in the sustained release of SORT1, which effectively downregulated GRN protein levels, suppressed M2 macrophage polarization and TGF-β feedback signaling, and significantly inhibited tumor growth in vivo. Collectively, our findings establish GRN as a promising therapeutic target and revealed that SORT1@HAMA could serve as a potential strategy for targeting the GBM tumor microenvironment.

Acknowledgements

This work was funded by the Natural Science Foundation of Gansu Province (No. 24JRRA-1109) and the National Natural Science Foundation of China (No. 82360566).

Disclosure of conflict of interest

None.

Address correspondence to: Yawen Pan, Lanzhou University Second Hospital, Lanzhou, Gansu, China. E-mail: panyawen2025@163.com

References

[1] Price M, Ballard CAP, Benedetti JR, Kruchko C, Barnholtz-Sloan JS and Ostrom QT. CBTRUS statistical report: primary brain and other central nervous system tumors diagnosed in the

united states in 2018-2022. Neuro Oncol 2025; 27: iv1-iv66.
[2] Wen PY, Weller M, Lee EQ, Alexander BM, Barnholtz-Sloan JS, Barthel FP, Batchelor TT, Bindra RS, Chang SM, Chiocca EA, Cloughesy TF, DeGroot JF, Galanis E, Gilbert MR, Hegi ME, Horbinski C, Huang RY, Lassman AB, Le Rhun E, Lim M, Mehta MP, Mellinghoff IK, Minniti G, Nathanson D, Platten M, Preusser M, Roth P, Sanson M, Schiff D, Short SC, Taphoorn MJB, Tonn JC, Tsang J, Verhaak RGW, von Deimling A, Wick W, Zadeh G, Reardon DA, Aldape KD and van den Bent MJ. Glioblastoma in adults: a Society for Neuro-Oncology (SNO) and European Society of Neuro-Oncology (EANO) consensus review on current management and future directions. Neuro Oncol 2020; 22: 1073-1113.
[3] Lowenstein PR. Oncostreams organize peritumoral glioma infiltration. Nat Cancer 2025; 6: 1485-1487.
[4] Faisal SM, Clewner JE, Stack B, Varela ML, Comba A, Abbud G, Motsch S, Castro MG and Lowenstein PR. Spatiotemporal insights into glioma oncostream dynamics: unraveling formation, stability, and disassembly pathways. Adv Sci (Weinh) 2024; 11: e2309796.
[5] Andersen BM, Faust Akl C, Wheeler MA, Chiocca EA, Reardon DA and Quintana FJ. Glial and myeloid heterogeneity in the brain tumour microenvironment. Nat Rev Cancer 2021; 21: 786-802.
[6] Dong D, Zhang W, Xiao W, Wu Q, Cao Y, Gao X, Huang L, Wang Y, Chen J, Wang W and Zhan Q. A GRN Autocrine-dependent FAM135B/AKT/mTOR feedforward loop promotes esophageal squamous cell carcinoma progression. Cancer Res 2021; 81: 910-922.
[7] Zhou T, Qian H, Zhang D, Fang W, Yao M, Shi H, Chen T, Chai C and Guo B. PGRN inhibits CD8(+)T cell recruitment and promotes breast cancer progression by up-regulating ICAM-1 on TAM. Cancer Immunol Immunother 2024; 73: 76.
[8] Tsuji S, Kudo U, Takahashi K, Nakamura S and Shimazawa M. The role of progranulin in macrophages of a glioblastoma model. J Neurooncol 2024; 170: 319-329.
[9] Caverzán MD, Beaugé L, Oliveda PM, Cesca González B, Buhler EM and Ibarra LE. Exploring monocytes-macrophages in immune microenvironment of glioblastoma for the design of novel therapeutic strategies. Brain Sci 2023; 13: 542.
[10] Lin C, Wang N and Xu C. Glioma-associated microglia/macrophages (GAMs) in glioblastoma: Immune function in the tumor microenvironment and implications for immunotherapy. Front Immunol 2023; 14: 1123853.
[11] Xu SM, Xiao HY, Hu ZX, Zhong XF, Zeng YJ, Wu YX, Li D and Song T. GRN is a prognostic biomarker and correlated with immune infiltration in glioma: a study based on TCGA data. Front Oncol 2023; 13: 1162983.
[12] Zhang W, Li L, Bian PP, Luo QP and Xiong ZT. PLEKHA4 is a prognostic biomarker and correlated with immune infiltrates in glioma. Biomed Res Int 2023; 2023: 4504474.
[13] Poniatowski ŁA, Woźnica M, Wojdasiewicz P, Mela-Kalicka A, Romanowska-Próchnicka K, Purrahman D, Żurek G, Krawczyk M, Nameh Goshay Fard N, Furtak-Niczyporuk M, Jaroszynski J, Mahmoudian-Sani MR and Joniec-Maciejak I. The role of progranulin (PGRN) in the pathogenesis of glioblastoma multiforme. Cells 2024; 13: 124.
[14] Bandey I, Chiou SH, Huang AP, Tsai JC and Tu PH. Progranulin promotes Temozolomide resistance of glioblastoma by orchestrating DNA repair and tumor stemness. Oncogene 2015; 34: 1853-1864.
[15] Miyakawa S, Sakuma H, Warude D, Asanuma S, Arimura N, Yoshihara T, Tavares D, Hata A, Ida K, Hori Y, Okuzono Y, Yamamoto S, Iida K, Shimizu H, Kondo S and Sato S. Anti-sortilin1 antibody up-regulates progranulin via sortilin1 down-regulation. Front Neurosci 2020; 14: 586107.
[16] Simon MJ, Logan T, DeVos SL and Di Paolo G. Lysosomal functions of progranulin and implications for treatment of frontotemporal dementia. Trends Cell Biol 2023; 33: 324-339.
[17] Shadab A, Farokhi S, Fakouri A, Mohagheghzadeh N, Noroozi A, Razavi ZS, Karimi Rouzbahani A, Zalpoor H and Mahjoor M. Hydrogel-based nanoparticles: revolutionizing brain tumor treatment and paving the way for future innovations. Eur J Med Res 2025; 30: 71.
[18] Lin J, Chen C, Li S, Chen L, Fang M, Fu S, Chen K, Xu H, Zhang F, Wang R, Jiang C, Tang M, Liu Z, Wang S, Liu K, Niu C, Li B, Liu X, Cheng C, Tang AH and Qu K. Spatial and single-cell characterization of human glioblastoma tumor microenvironment reveals malignant cellular communities. Nat Neurosci 2026; [Epub ahead of print].
[19] Nielsen SR, Quaranta V, Linford A, Emeagi P, Rainer C, Santos A, Ireland L, Sakai T, Sakai K, Kim YS, Engle D, Campbell F, Palmer D, Ko JH, Tuveson DA, Hirsch E, Mielgo A and Schmid MC. Macrophage-secreted granulin supports pancreatic cancer metastasis by inducing liver fibrosis. Nat Cell Biol 2016; 18: 549-560.
[20] Yang D, Wang LL, Dong TT, Shen YH, Guo XS, Liu CY, Liu J, Zhang P, Li J and Sun YP. Progranulin promotes colorectal cancer proliferation and angiogenesis through TNFR2/Akt and

ERK signaling pathways. Am J Cancer Res 2015; 5: 3085-3097.
[21] Dong Y, Tan H, Wang L and Liu Z. Progranulin promoted the proliferation, metastasis, and suppressed apoptosis via JAK2-STAT3/4 signaling pathway in papillary thyroid carcinoma. Cancer Cell Int 2023; 23: 191.
[22] Koo DH, Lee KS, Sim SH, Chae H, Lee EG, Han JH, Jung SY, Lee S, Kang HS, Lee ES, Park CY and Oh SW. Progranulin and breast cancer mortality: 13-year follow-up of a cohort study. Breast Cancer (Dove Med Press) 2023; 15: 251-261.
[23] Chen S, Bie M, Wang X, Fan M, Chen B, Shi Q and Jiang Y. PGRN exacerbates the progression of non-small cell lung cancer via PI3K/AKT/Bcl-2 antiapoptotic signaling. Genes Dis 2021; 9: 1650-1661.
[24] Yoo S, Patel AS, Karam S, Zhong Y, Wang L, Jiang F, Kong R, Bikvan S, Wang W, Sinha A, Powell CA, Zhu J and Watanabe H. Transcriptional regulatory network analysis identifies GRN as a key regulator bridging chemotherapy and immunotherapy response in small cell lung cancer. J Hematol Oncol 2025; 18: 14.
[25] Purrahman D, Mahmoudian-Sani MR, Saki N, Wojdasiewicz P, Kurkowska-Jastrzębska I and Poniatowski ŁA. Involvement of progranulin (PGRN) in the pathogenesis and prognosis of breast cancer. Cytokine 2022; 151: 155803.
[26] Xu L, Mo Y, Yu B and Fan S. BRD8 inhibits colorectal cancer progression through TGF-beta1-mediated tumor-associated macrophage recruitment. Discov Oncol 2025; 16: 1419.
[27] Liu L, Li Y and Li B. Interactions between cancer cells and tumor-associated macrophages in tumor microenvironment. Biochim Biophys Acta Rev Cancer 2025; 1880: 189344.
[28] Huang W, Fu B and Xu H. beta-elemene inhibits tumor-promoting in small cell lung cancer by affecting M2 macrophages and TGF-beta. BMC Pulm Med 2025; 25: 97.
[29] Liao Y, Zhang W, Liu Y, Zhu C and Zou Z. The role of ubiquitination in health and disease. MedComm (2020) 2024; 5: e736.
[30] Cabrera PV, Blanco G, Alaniz L, Greczanik S, Garcia M, Alvarez E and Hajos SE. CD44 and hyaluronic acid regulate in vivo iNOS expression and metalloproteinase activity in murine air-pouch inflammation. Inflamm Res 2004; 53: 556-566.

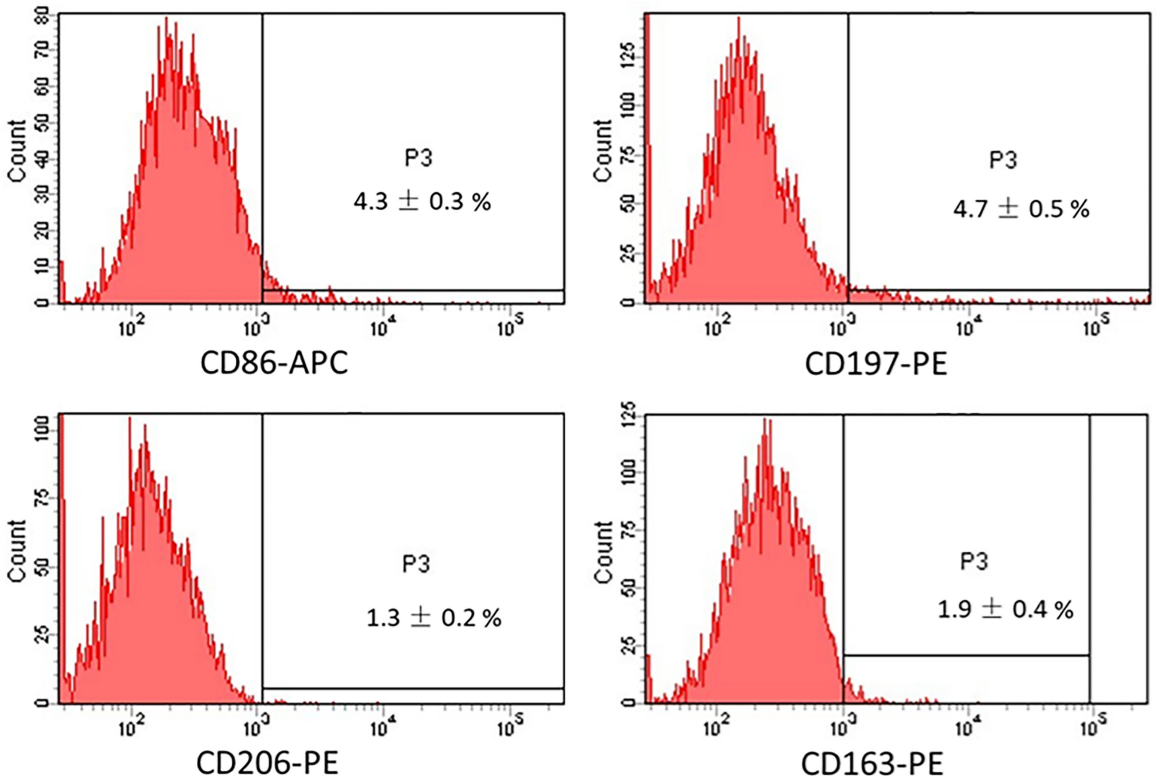

Figure S1. Identification of M0 macrophages. Flow cytometry analysis showed that in primary human peripheral blood macrophages, the proportions of CD86, CD197, CD206, and CD163 positive cells were all below 5%.

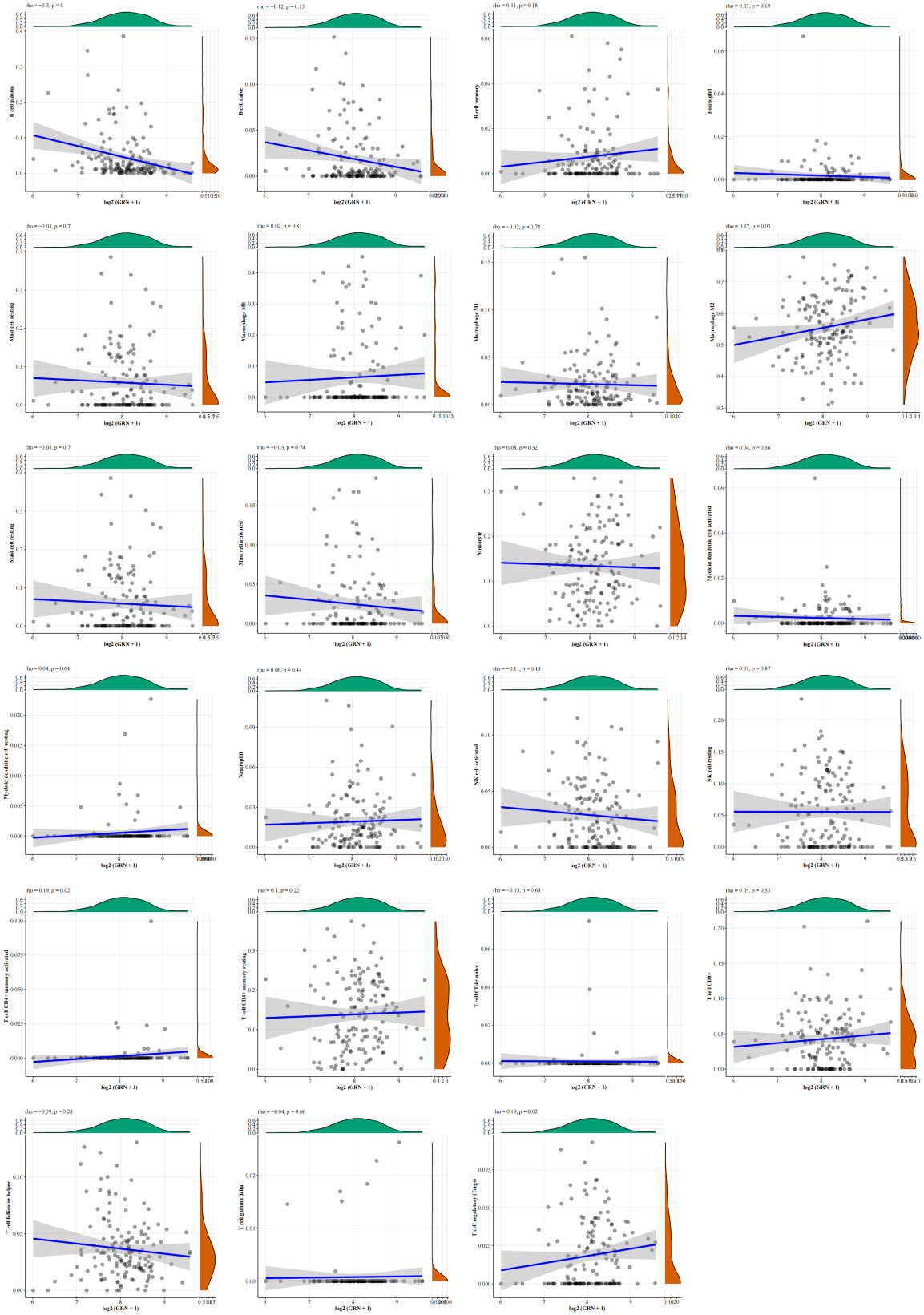

Figure S2. The complete CIBERSORT output results and the correlation heatmap.

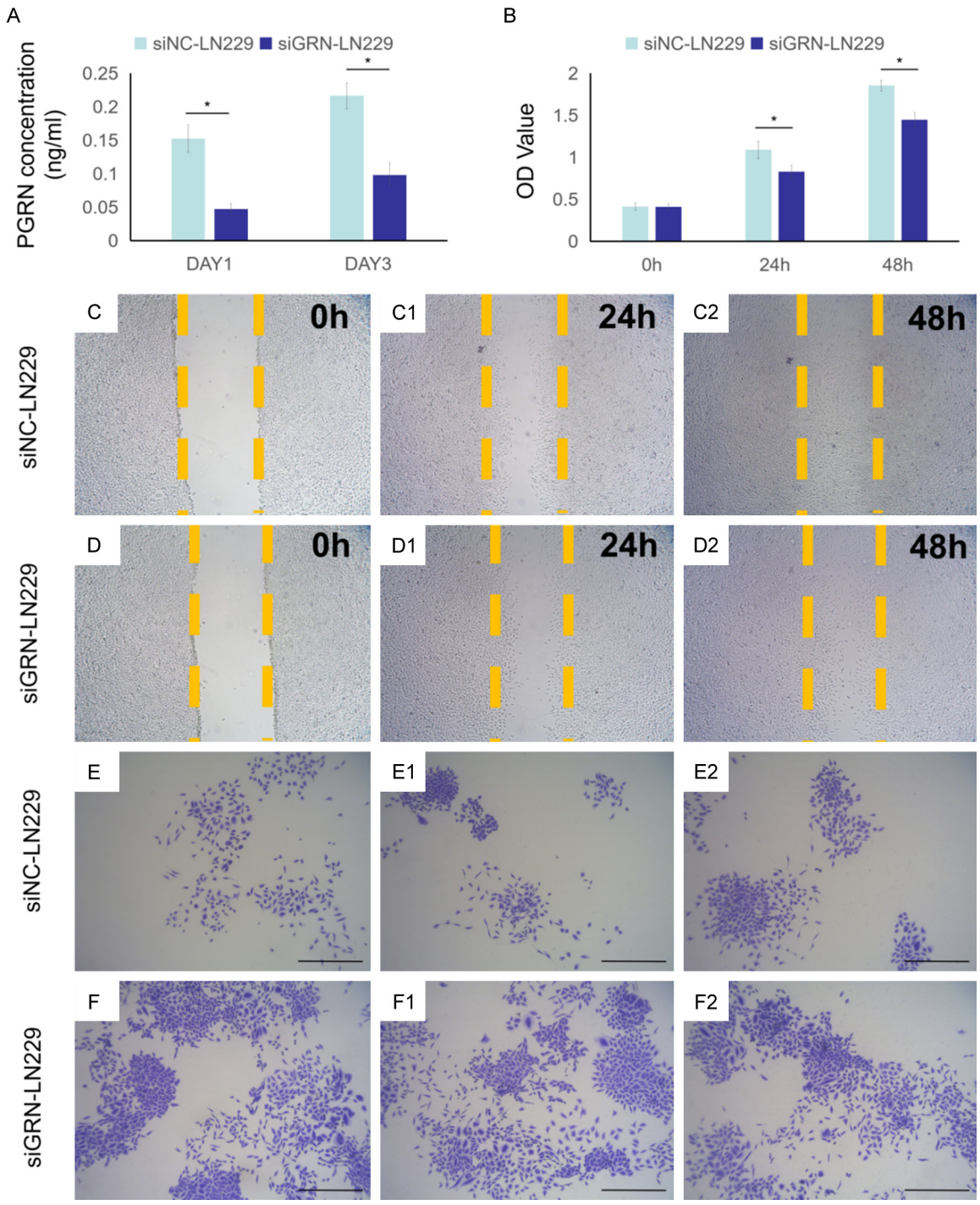

Figure S3. GRN knockdown suppresses the malignant phenotypes of GBM cells (LN229). A. The level of GRN secreted by siNC- and siGRN-transfected LN229 was quantified using ELISA. B. The effect of GRN knockdown on LN229 cell proliferation was assessed using a CCK-8 assay. C-D2. Wound healing assays were performed at 0, 24, and 48 h to evaluate the effect of GRN knockdown on the migration of LN229 cells. E-F2. The effects of GRN knockdown on the clonogenic and tumorigenic potential of LN229 cells were determined using single-cell colony formation assays. Scale bar: 250 μm.

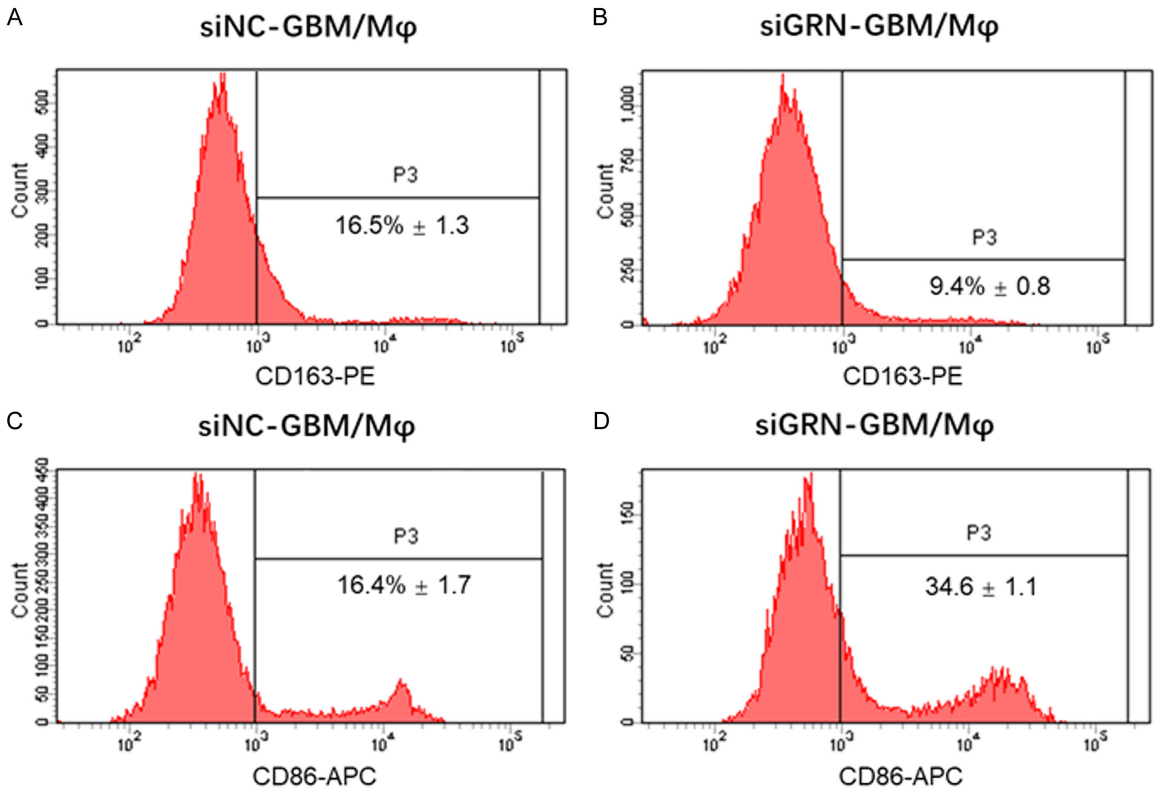

Figure S4. Supplementary analysis of macrophage typing. A-D. Flow cytometry analysis revealed an increase in the number of M1 macrophages ($CD86^+$) and a decrease in the number of M2 macrophages ($CD163^+$) in the coculture with siGRN-GBM cells.